JOURNAL OF COLLOID AND INTERFACE SCIENCE **186,** 118–128 (1997)
ARTICLE NO. CS964624

Spectroscopic Evidence for the Formation of Mixed-Cation Hydroxide Phases upon Metal Sorption on Clays and Aluminum Oxides

ANDRÉ M. SCHEIDEGGER,*[,1] GERALDINE M. LAMBLE,† AND DONALD L. SPARKS*

**Department of Plant and Soil Sciences, University of Delaware, Newark, Delaware 19717-1303; and †Building 510E, Brookhaven National Laboratory, Upton, New York 11973*

Received June 20, 1996; accepted October 2, 1996

Retention of heavy metal ions on soil mineral surfaces is an important process for maintaining environmental quality. A thorough understanding of the kinetics and mechanisms of heavy metal sorption on soil mineral surfaces is therefore of fundamental importance. The present study examines the kinetics and mechanisms of Ni(II) sorption onto pyrophyllite, kaolinite, gibbsite, and montmorillonite. Ni sorption reactions were initially fast (15–40% of the initial Ni was removed within the first hour). Thereafter, the rate of sorption decreased significantly. X-ray absorption fine structure (XAFS) spectroscopy was used to determine the local structural environment of Ni(II). Data analysis reveals the presence of polynuclear Ni surface complexes. Ni–Ni bond distances (3.00–3.03 Å) were distinctly shorter than in $Ni(OH)_2$(s) (3.09 Å). We propose that the reduction of the Ni-Ni distances is caused by the formation of mixed Ni/Al hydroxide phases. The XAFS spectra and derived structural parameters are similar to those in takovite ($Ni_6Al_2(OH)_{16}CO_3 \cdot H_2O$), thus suggesting the presence of a Ni phase of similar structure. Even though dissolved Al could not be detected in our samples, Al could have been released into solution and incorporated into mixed Ni/Al hydroxide-like phases. The formation of such phases can explain the finding that the dissolution rates (Si-release) are strongly enhanced (relative to the dissolution rates of the clays alone) as long as Ni sorption is pronounced. We suspect that the release of Al into solution is the rate-determining step for the formation of mixed Ni/Al hydroxide-like phases in our study. Our study demonstrates that mixed Ni/Al hydroxide-like compounds can form when Ni is introduced into a suitable environment in which there is a source of hydrolyzed species of Al. One can speculate that the formation of mixed-cation hydroxide compounds also represents a plausible ''sorption mode'' for other divalent metal ions when silicates or oxides are present. It has been shown that similar mixed-cation hydroxide compounds can be synthesized when Mg(II), Ni(II), Co(II), Zn(II), or Mn(II) is added to suspensions containing Al(III), Fe(III), and Cr(III). Thus, the formation of mixed-cation hydroxide compounds should be considered when conducting metal sorption experiments, modeling metal surface complexation, determining speciation, and assessing the risk of the migration of contaminants in polluted sites.

Key Words: **XAFS; sorption; surface precipitation; kinetics.**

INTRODUCTION

Sorption reactions at solid–water interfaces decrease solute mobility and often control the fate, bioavailability, and transport of trace metal ions such as Zn, Cd, Pb, Ni, and Cu in aquatic and soil environments. Correctly determining the sorption mechanisms of metals on clay and other mineral surfaces is important for understanding the fate of such pollutants in contaminated soils and sediments and will facilitate successful environmental remediation procedures.

Most of the research on metal sorption on mineral surfaces has been studied from a macroscopic, equilibrium approach. The focus has been mainly on the determination of distribution coefficients based on a 24 h reaction time. Natural aquatic and terrestrial systems are, however, seldom, if ever, at equilibrium (1). Studies on the kinetics of heavy metal sorption on clay and oxide surfaces reveal that sorption reactions are typically rapid initially, occurring on time scales of minutes or hours, and then the rates diminish gradually, over time scales of days or weeks. The rapid stage is normally interpreted as an adsorption phenomenon (1, 2). There are several interpretations of the slow reaction stage. Benjamin and Leckie (3) and Dzombak and Morel (4) attribute the slow sorption kinetics on mineral surfaces to adsorption onto sites of lower reactivity. In most cases the decline in reaction rate is regarded as nonhomogenous and has been explained by diffusion of the adsorbate into the adsorbent (5) or by a precipitation reaction (6). However, it is not possible to discriminate among the suggested sorption mechanisms without spectroscopic evidence (7).

Recent studies using surface spectroscopic and microscopic techniques such as X-ray absorption fine structure (XAFS) spectroscopy have demonstrated that the formation of surface precipitates is a far more important process than previously thought (8–15). Using XAFS, the nucleation of heavy metals on clay and oxide surfaces has been observed at metal surface loadings far below a theoretical monolayer coverage, and in a pH range well below that at which metal hydroxide precipitates would be expected to form according to the thermodynamic solubility product (8, 11, 12, 14, 15). Possible causes of this such as enhanced surface concentra-

[1] To whom correspondence should be addressed.

0021-9797/97 $25.00

tion, reduction of the dielectric constant of water near the surface, and solid solution formation (solid phase in which a trace ion lowers its solubility by co-precipitation into another compound) have been discussed (12, 16).

Previous studies on Ni sorption on pyrophyllite revealed that the sorption behavior distinctively changed when the reaction pH was increased above 7 (17, 18). As an example, a strong decrease in the sorption rates in the higher pH-regime was observed. The decrease was attributed to slow nucleation processes occurring on the pyrophyllite surface even at reaction conditions undersaturated with respect to the formation of $Ni(OH)_2$(s) in homogenous solution (15, 17). The present study examines the kinetics and mechanisms of Ni(II) sorption on pyrophyllite, kaolinite, gibbsite, and montmorillonite at pH 7.5. XAFS spectroscopy is used to determine the local atomic environment of sorbed Ni(II). Derived structural parameters are then compared with those of reference compounds, and possible sorption modes are discussed on the basis of kinetic and spectroscopic data.

The Ni^{2+} cation, like many other metal ions (e.g., Co^{2+}, Cd^{2+}, Pb^{2+}, Mn^{2+}, Cu^{2+}, Zn^{2+}, and Cr^{3+}), has a tendency to be adsorbed specifically on clay and oxide surfaces and to hydrolyze within common environmental pH ranges (pH 3–9) (15, 19, 20). Kaolinite and pyrophyllite were selected because they represent 1:1 and 2:1 clays which have no structural charge in their pure stoichiometric form ($Al_2Si_2O_5(OH)_4$ and $Al_2Si_4O_{10}(OH)_2$, respectively). Sorption of aqueous species and development of surface charge are controlled mainly by amphoteric reactions at oxygen sites on aluminol and siloxane surfaces that are conceptually similar to surface reactions on oxide minerals (1, 21). Pyrophyllite shows little deviation from the ideal chemical formula. A very small substitution of Al for Si can occur which is commonly ~0.001 Al cations per formula unit (22). Natural kaolinites do, however, have a small cation-exchange capacity (1–15 cmoles/kg (16)). Montmorillonite represents a more complex surface than kaolinite and pyrophyllite and has both external and internal binding sites. Gibbsite ($Al(OH)_3$) is an important Al oxide mineral in soils. Specific sorption on strongly pH-dependent surface sites is considered to account for the binding of metal ions by the gibbsite surface (2, 16).

EXPERIMENTAL METHODS

Materials. The <2 μm clay fraction of well-characterized kaolinite, pyrophyllite, and Ca-montmorillonite were used. The preparation and characterization of the minerals are described elsewhere (15, 23, 24). We also used gibbsite. X-ray diffraction (XRD, Philips, PW1729) analysis revealed that the material contains 10% bayerite, a polymorph of gibbsite. Particle size analysis showed that 90% of the material is less than 2 μm. The specific surface area of the materials was determined by the BET method using N_2 adsorption (kaolinite, pyrophyllite, and gibbsite) and the ethylene glycol monoethyl ether (EGME) method (25) (montmorillonite). The surface areas were 25 m^2/g for gibbsite, 15 m^2/g for kaolinite, 96 m^2/g for pyrophyllite, and 520 m^2/g for montmorillonite.

Batch studies. Ni sorption samples were prepared using a batch technique designed to maintain constant pH (pH-stat, Radiometer) and temperature (298 K) and to eliminate CO_2 by purging with N_2. The sorbents were hydrated in a 0.1 *M* $NaNO_3$ solution for 24 h prior to reaction with Ni. After hydration the pH of the suspension was adjusted to pH 7.5 with 0.1 *M* NaOH and the mixture was brought to a solid/liquid ratio of 10 g/liter. Ni from a 0.1 *M* $Ni(NO_3)_2$ stock solution was dispensed in stepwise additions (within ~5 min) in order to avoid the formation of Ni precipitates due to local oversaturation of the suspension. The pH was automatically held constant (pH 7.5) and the electrode recalibrated every 24 h. The initial Ni concentration (3 m*M*) and the reaction pH (7.5) were selected to achieve considerable sorption densities and to ensure that the bulk solutions were undersaturated with respect to crystalline $Ni(OH)_2$. Samples were centrifuged, and the supernatant was passed through a 0.22 μm membrane filter and analyzed by inductively coupled plasma emission (ICP) spectrometry for Ni, Al, and Si. The remaining wet pastes were washed with excess high-purity water to adequately remove entrained electrolyte and then centrifuged again. The washing process was repeated twice and resulted in no significant Ni desorption. The samples were then sealed and stored in a refrigerator to keep them moist for XAFS analysis.

XAFS studies. X-ray absorption fine structure spectra were recorded at beamline X-11A at the NSLS (Brookhaven National Laboratory, Upton, NY). A Si (111) crystal was employed in the monochromator. Beam energy was calibrated by assigning the first inflection on the K absorption edge of a nickel metal foil to an energy of 8333 eV. The spectra were collected in fluorescence mode using a Stern–Heald-type detector (26) which is available commercially (The EXAFS Co.) and known as a Lytle detector (27). The spectra were run at 77K to reduce dampening of the XAFS oscillation by thermal disorder. Comparisons of spectra recorded at 77K and room temperature revealed no change in structural information, while the signal-to-noise ratio was maximized by lowering the temperature (8, 11, 14). Details on the experimental setup can be found elsewhere (15).

Reference compounds ($Ni(OH)_2$ (Johnson Mattey Co), Ni_2Si (Johnson Mattey Co.), and takovite ($Ni_6Al_2(OH)_{16}CO_3 \cdot H_2O$, Kambalda W.A., Australia)) were lightly crushed to powders with an agate mortar and pestle and diluted with boron nitride to obtain a 1 wt % mixture.

Data analysis was accomplished using the program EXCURVE (28). The background of the spectra was subtracted using a cubic spline fit technique. After normalization the raw absorption data were converted from energy to *k* space and weighted by k^2 in order to compensate for the damping

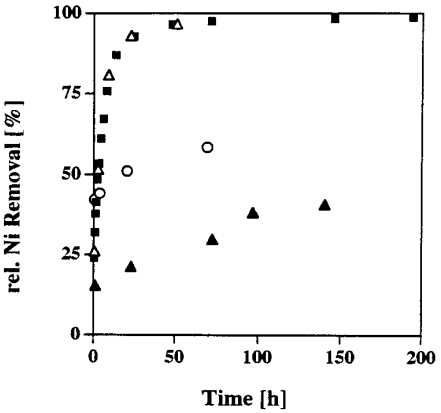

FIG. 1. Kinetics of Ni sorption (%) on pyrophyllite (■), kaolinite (△), gibbsite (▲), and montmorillonite (○) from a 3 m*M* Ni solution at pH 7.5 and an ionic strength $I = 0.1$ *M* ($NaNO_3$). The last sample of each experiment was collected and analyzed by XAFS.

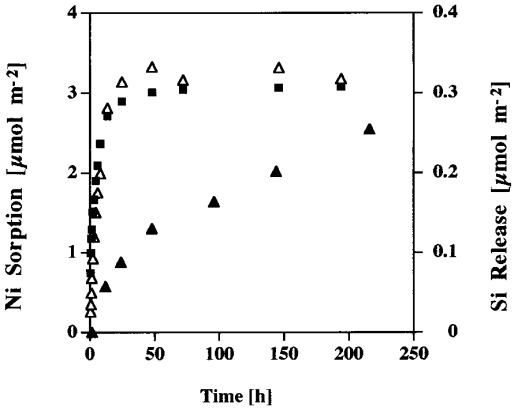

FIG. 2. The kinetics of Ni sorption on pyrophyllite from a 3 m*M* M Ni solution at pH 7.5. (■) denotes the amount of sorbed Ni (μmol m^{-2}) and (△) the amount of simultaneous dissolved Si (μmol m^{-2}). The dissolution of untreated pyrophyllite at pH 7.5 is shown for comparison (▲).

of the XAFS amplitude with increasing *k*. The zero energy point, E_0, was taken as the edge inflection point and was treated as an adjustable fitting parameter. Amplitude parameters and phase shifts for Ni, O, and Si/Al were obtained experimentally from the spectra of crystalline $Ni(OH)_2$ and Ni_2Si. Successive shells were isolated in the Fourier-transformed spectra, back-transformed, and fitted in *k* space by adjustment of the zero energy point (E_0), the interatomic distances (*R*'s), coordination number (*N*'s), and Debye–Waller-type terms, until a best fit was obtained between the predicted and experimental curves. Fitting was done using data in the *k* range 3.4–14.2 $Å^{-1}$. After the structural parameters for each successive shell were obtained out to ~3.9 Å, the structural parameters were then combined to model the Fourier-filtered spectrum. Errors given were estimated on the basis of the fitting results. The *R* values were accurate to ±0.02 Å, and the *N* values were accurate to ±20% for O and Ni and ±40% for Si/Al.

RESULTS

Ni sorption kinetics. Figure 1 illustrates the kinetics of Ni sorption on pyrophyllite, kaolinite, gibbsite, and montmorillonite from a 3 m*M* Ni solution at pH = 7.5. It reveals that for kaolinite and pyrophyllite relative Ni removal from solution follows a similar sorption trend with ≈90% Ni sorbed within the first 24 h. At the end of the experiments, relative Ni removal from solution is almost complete (Ni/kaolinite system, 97% sorbed after 70 h; Ni/pyrophyllite system, 98% sorbed after 200 h). Ni sorption on gibbsite and montmorillonite exhibits a fast initial step. Thereafter, relative Ni removal from solution distinctively slows down. Relative Ni sorption increases from 42% to 58% for the Ni/montmorillonite system (time range 0.5–70 h) and from 15% to 41% for the Ni/gibbsite system (time range 1–140 h). The latter data set indicates a linear sorption behavior for the second sorption step. We suspect that several more days or weeks would be required for Ni sorption on gibbsite to be completed.

Figures 2–4 illustrate the kinetics of Ni sorption on pyrophyllite, kaolinite, and montmorillonite (data from Fig. 1 except Ni/gibbsite) and of dissolved Si from these Ni-treated minerals during the experiments. The data are expressed in μmol m^{-2} vs time. Si data were corrected for the small Si concentrations ($<1 \times 10^{-4}$ *M*) present in solution at the beginning of the experiments due to the preceding hydration process of the clays.

Figure 2 reveals that the release of Si into solution exhibits a similar kinetic behavior as Ni sorption on pyrophyllite. When one compares the Si release rate with the dissolution rate of the clay alone (Ni-untreated pyrophyllite), the Si release rate in the Ni-treated system is strongly enhanced as long as Ni removal from solution is pronounced (Fig. 2). However, the overall Si release rates from Ni-treated and Ni-untreated pyrophyllite during the

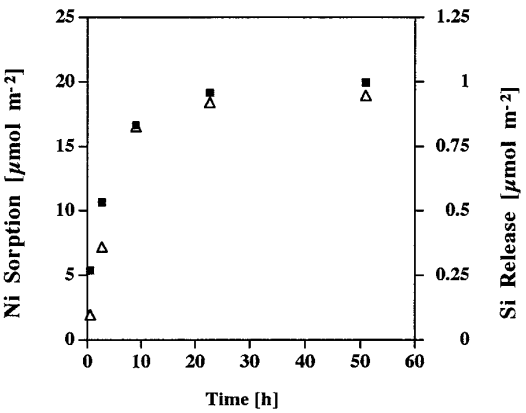

FIG. 3. The kinetics of Ni sorption on kaolinite from a 3 m*M* Ni solution at pH 7.5. (■) denotes the amount of sorbed Ni (μmol m^{-2}) and (△) the amount of simultaneous dissolved Si (μmol m^{-2}).

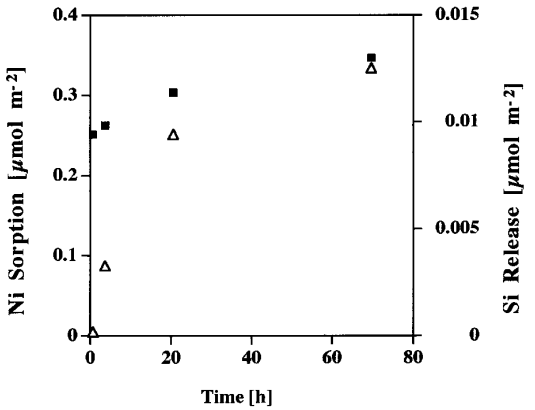

FIG. 4. The kinetics of Ni sorption on montmorillonite from a 3 m*M* Ni solution at pH 7.5. (■) denotes the amount of sorbed Ni (μmol m^{-2}) and (△) the amount of simultaneous dissolved Si (μmol m^{-2}).

experiment were similar. The dissolution rates were 3.2×10^{-13} mol m^{-2} s^{-1} (pH 7.5, time range 0–216 h) for Ni-untreated pyrophyllite and 4.6×10^{-13} mol m^{-2} s^{-1} (pH 7.5, time range 0–194 h) for Ni-treated pyrophyllite. The predominant Si specie in solution at pH 7.5 is monosilic acid ($Si(OH)_4$, pK_1 = 9.46). The concentration of $SiO(OH)_3^-$ (≈1%) is low. Equilibrium diagrams of amorphous silica reveal that at pH 7.5 the concentrations of multinuclear silica species such as $Si_4O_6(OH)_6^{2-}$ and $SiO_2(OH)_2^{2-}$ are negligible (29).

Figure 3 exhibits a similar correlation between Ni sorption and Si release for the Ni/kaolinite system. Si release is pronounced as long as Ni sorption is pronounced and decreases when Ni sorption decreases. The Si release rate during the experiment was 5.2×10^{-12} mol m^{-2} s^{-1} (pH 7.5, time range 0–51 h) and higher than the dissolution rate given in the literature for kaolinite alone (2.5×10^{-13} mol m^{-2} s^{-1}, pH 6.5 (30), and 5×10^{-14} mol m^{-2} s^{-1}; pH 7.5 (31)).

For the Ni/montmorillonite system a correlation between the kinetics of Ni sorption and the release rate of Si is not evident (Fig. 4). 72% of the total Ni removed from solution during the experiment is sorbed within the first 30 min. Si release during this first reaction stage is negligible. The Si release rate over the course of the entire experiment is 3.2×10^{-14} mol m^{-2} s^{-1} (pH 7.5, time range 0–70 h) and is comparable to the dissolution rate of montmorillonite found in the literature (4×10^{-14} mol m^{-2} s^{-1}, pH 5 (32), and 1×10^{-15} mol m^{-2} s^{-1}, pH 6 (33)).

We could not determine the dissolution rate of the Ni/gibbsite system since the [Al] in solution was too low (<50 ppb) to produce reliable ICP measurements. The measurement of the dissolution rates of aluminum oxides at pH 7.5 would require the addition of organic agents which readily complex aluminum and prevent the precipitation of an aluminum hydroxide phase (31). Dissolution rate of aluminum oxides at neutral pH found in the literature are therefore rare (3×10^{-14} mol m^{-2} s^{-1} for α-Al_2O_3, pH 7.5 (31)).

XAFS study. Figure 5 shows normalized, background-subtracted and *k*-weighted XAFS spectra of Ni sorbed on pyrophyllite, kaolinite, gibbsite, and montmorillonite. The XAFS samples were collected at the end of the Ni sorption experiments (see Experimental Methods). The corresponding surface sorption densities, Γ's, were 3.1 μmol m^{-2} for pyrophyllite, 19.9 μmol m^{-2} for kaolinite, 5.0 μmol m^{-2} for gibbsite, and 0.35 μmol m^{-2} for montmorillonite (Table 1). The spectra of crystalline $Ni(OH)_2$ and takovite are shown for comparison. One can observe a strong XAFS out to higher energies, which indicates the presence of heavy backscatterer elements such as Ni. The figure reveals that there is an obvious similarity among the spectra of Ni sorption samples and the spectrum of takovite.

Figure 6 illustrates radial structure functions (RSFs) produced by forward Fourier transforms of the XAFS spectra represented in Fig. 5. The spectra were uncorrected for phase shift. All spectra showed a peak at $R \approx 1.8$ Å, which represents the first coordination shell of Ni. A second peak representing the second Ni shell can be observed at $R \approx 2.8$ Å in the spectra of the Ni sorption samples and takovite (Fig. 6). The figure also shows peaks beyond the second shell at $R \approx 5$–6 Å. These peaks resulted from multiple scattering among Ni atoms (12, 14) and will not be discussed further.

The structural parameters derived from XAFS analysis are summarized in Table 1. Least-squares fits of filtered XAFS of the first RSF peak reveal that in the first coordination shell Ni is surrounded by six O atoms. This behavior indicates that Ni(II) is in an octahedral environment. The Ni–O distances for the Ni sorption samples are 2.02–2.03 Å and similar to those in takovite (2.03 Å, this study and (34)). The Ni–O distances in crystalline $Ni(OH)_2$(s) are distinctly longer (2.06 Å, this study; 2.05 Å (35); 2.07 Å (36)).

For the second shell, best fits were obtained by including both Ni and Si or Al as second-neighbor backscatterer atoms (see discussion Fig. 8). Because Si and Al differ in atomic number by 1 (Z = 14 and 13, respectively), backscattering is similar. They cannot be easily distinguished from each other as second-neighbor backscatterers, especially in circumstances such as this where the contribution of both is small and cannot be resolved from each other in the Fourier transform.

For the Ni sorption samples data analysis reveals 2.8 (montmorillonite) to 5.0 (gibbsite) Ni second-neighbor (N) atoms, indicative of the presence of polynuclear Ni surface complexes (see Table 1). No correlation between the Ni surface sorption densities, Γ's, and the N's of the Ni sorption samples is evident. Observed Ni–Ni distances (3.00–3.03 Å) are similar to those in takovite (3.01 Å, this study; 3.03 Å (34); 3.05 Å (37, 38)), but distinctly shorter (0.06–0.08 Å) than those in crystalline $Ni(OH)_2$(s) (3.09 Å, this study and (35)). XAFS data also reveal the presence of 1.8–2.7 Si/Al second-neighbor atoms at 3.02–3.07 Å. Again, the bond distances are in a good agreement with the Ni–Al

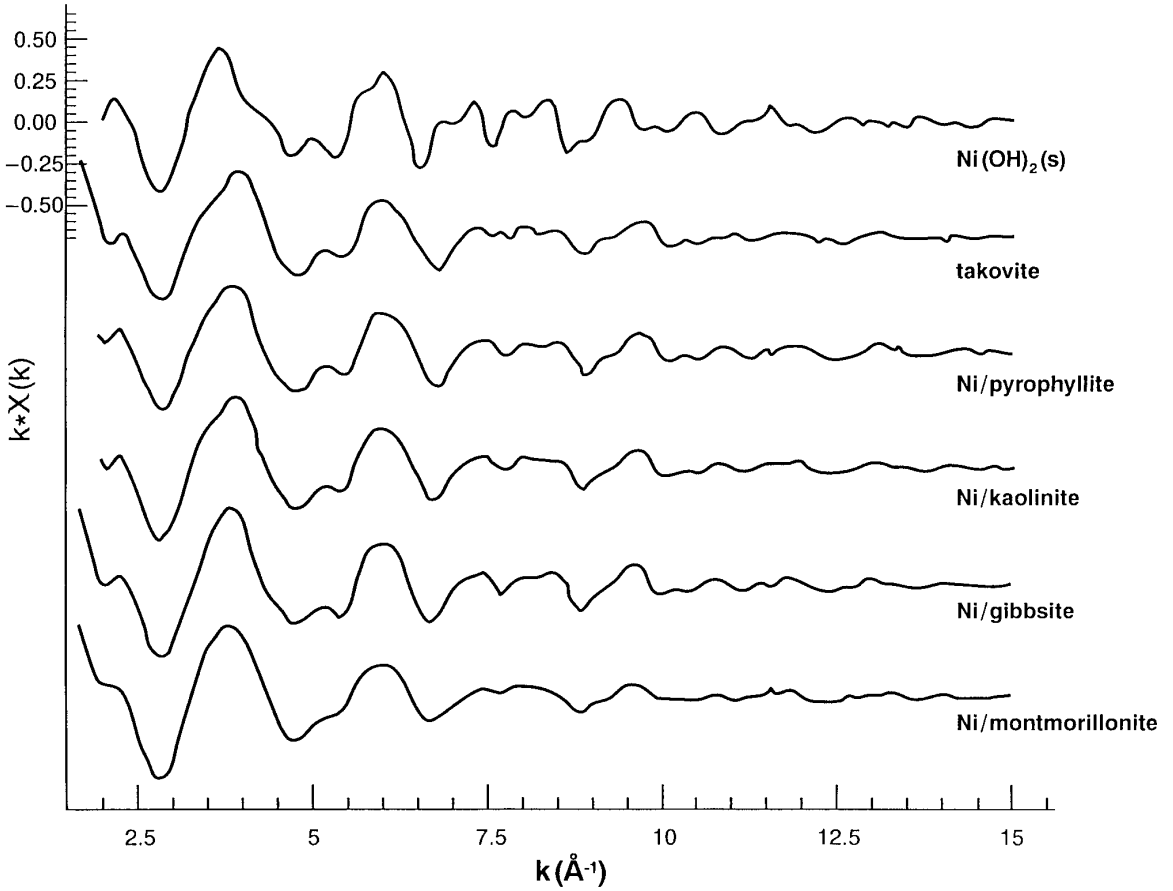

FIG. 5. *k*-Weighted, normalized, background-subtracted XAFS spectra of Ni sorbed on pyrophyllite, kaolinite, gibbsite, and montmorillonite compared to the spectrum of crystalline $Ni(OH)_2$(s) and takovite.

distances observed in takovite (3.03 Å, this study and (34); 3.05 Å (37, 38)).

Figure 7 shows a comparison of k^2-weighted XAFS functions for the Fourier back-transformed spectra to the theoretical spectra derived with parameters from analysis of the isolated shells. A good agreement between the Fourier back-transformed XAFS function and the theoretical fit is observable. The XAFS spectra of the Ni-treated sorption samples and the spectrum of takovite, our mixed Ni/Al hydroxide reference compound, appear to be almost identical.

Figure 8 illustrates that the XAFS spectra are best described by a fit that includes both Ni and Si/Al as second-neighbor backscatterer atoms. The figure shows the k^2-weighted filtered experimental XAFS spectra (solid line) in comparison with theoretical spectra (dashed line) of the second RSF peak of the Ni/pyrophyllite sample presented in

TABLE 1
Structural Information Derived from XAFS Analysis Using EXCURVE (28)

	Γ	Ni−O			Ni−Ni			Ni−Si/Al			
	(μmol/m^2)	R (Å)	N	$2\sigma^2$	R (Å)	N	$2\sigma^2$	R (Å)	N	$2\sigma^2$	N(Ni)/N(Si/Al)
$Ni(OH)_2$		2.06	6.0	0.011	3.09	6.0	0.010				
Takovite		2.03	6.0	0.01	3.01	3.1	0.009	3.03	1.1	0.009	2.8
Pyrophyllite	3.1	2.02	6.1	0.01	3.00	4.8	0.009	3.02	2.7	0.009	1.8
Kaolinite	19.9	2.03	6.1	0.01	3.01	3.8	0.009	3.02	1.8	0.009	2.2
Gibbsite	5.0	2.03	6.5	0.01	3.02	5.0	0.009	3.05	1.8	0.09	2.7
Montmorillonite	0.35	2.03	6.3	0.01	3.03	2.8	0.011	3.07	2.0	0.015	1.4

Note. Interatomic distances (R, Å), coordination numbers (N), and Debye–Waller factors ($2\sigma^2$, Å^2). The reported values are accurate to within $R \pm 0.02$ Å, $N_{(Ni-O)} \pm 20\%$, $N_{(Ni-Ni)} \pm 40\%$, and $N_{(Ni-Si/Al)} \pm 40\%$.

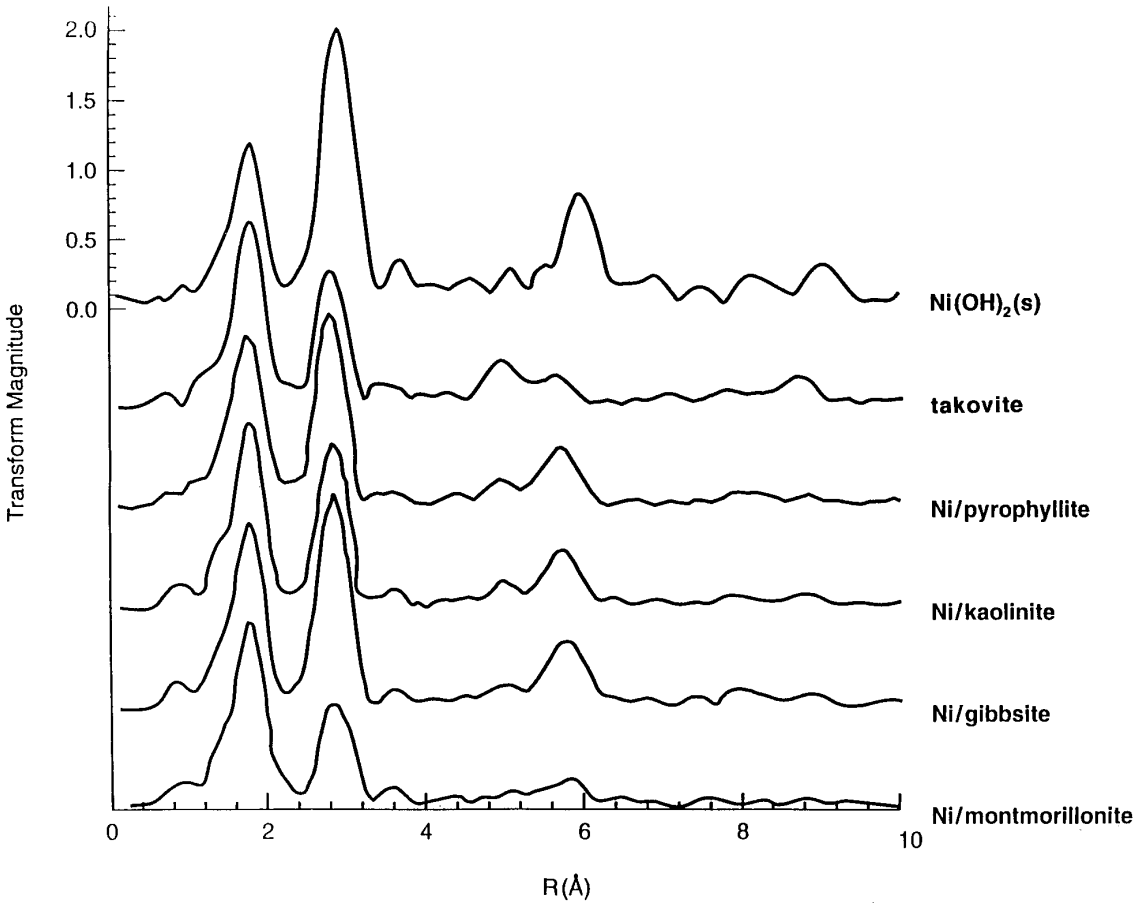

FIG. 6. Radial structure functions (RSFs) produced by forward Fourier transforms of Ni sorbed on pyrophyllite, kaolinite, gibbsite, and montmorillonite compared to the spectrum of crystalline $Ni(OH)_2$(s) and takovite. The spectra are uncorrected for phase shift.

Fig. 6. When both Ni and Si/Al are considered as second-neighbor backscatterer atoms, a good agreement between the Fourier back-transformed XAFS function and the fit is observable (Fig. 8a). The contribution of Ni (dashed line in Fig. 8b) and Si/Al (dashed line in Fig. 8c) to the best fit (dashed line in Fig. 8a) are shown in Fig. 8b and 8c, respectively. The best fit amplitude (dashed line in Fig. 8a) is smaller than the Ni amplitude alone (dashed line in Fig. 8b) because of the significant destructive interference by the Si or Al contribution (dashed line in Fig. 8c).

We also tried to fit the second RSF peak with Ni alone. The best fit is shown in Fig. 8d (fixed Debye–Waller factor, $2\sigma^2 = 0.009$). The obtained number of second shell neighbor atoms was significantly reduced ($N_{(\mathrm{Ni-Ni})} = 3.3$ at 2.99 Å). The figure reveals that Si/Al is required to produce a good fit (compare agreement between fit and experimental spectrum in Fig. 8a and 8d). There is a poor agreement between the Ni-alone fit (dashed line in Fig. 8d) and the experimental XAFS (solid line in Fig. 8d) in the low *k*-range (<6 Å) as well in the high *k*-range (>10 Å). Si/Al contributes strongly to the earlier region of the spectra (dashed line in Fig. 8c) and so its phase, which is partly out of phase with the Ni phase (dashed line in Fig. 8b), makes a strong contribution to alter the overall phase (dashed line in Fig. 8a) which Ni-alone could never mimic (dashed line in Fig. 8d). The errors in the high *k*-range are large, although the Si/Al contribution is smaller in amplitude. The Si/Al contribution is exactly out of phase with the Ni contribution and as a result there is a significant difference in amplitude.

DISCUSSION

The formation of polynuclear surface complexes. The study reveals that Ni sorption on pyrophyllite, kaolinite, gibbsite, and montmorillonite at pH 7.5 results in formation of polynuclear surface complexes. We observe the formation of surface species containing Ni clusters from solutions which are undersaturated with respect to the thermodynamic solubility product of $Ni(OH)_2$(s). Ni speciation using a chemical equilibrium speciation program which is based on a thermodynamic database (Environmental Simulation Program, OLI Systems, Morristown, NJ) reveals that Ni(II) is predominately present as Ni^{2+}(aq) (≈90%) and to a minor extent as $NiNO_3^-$(aq) (≈10%). The concentrations of hydrolysis products such as $Ni(OH)^+$, $Ni_4(OH)_4^{4+}$, $Ni_2(OH)^{3+}$, and

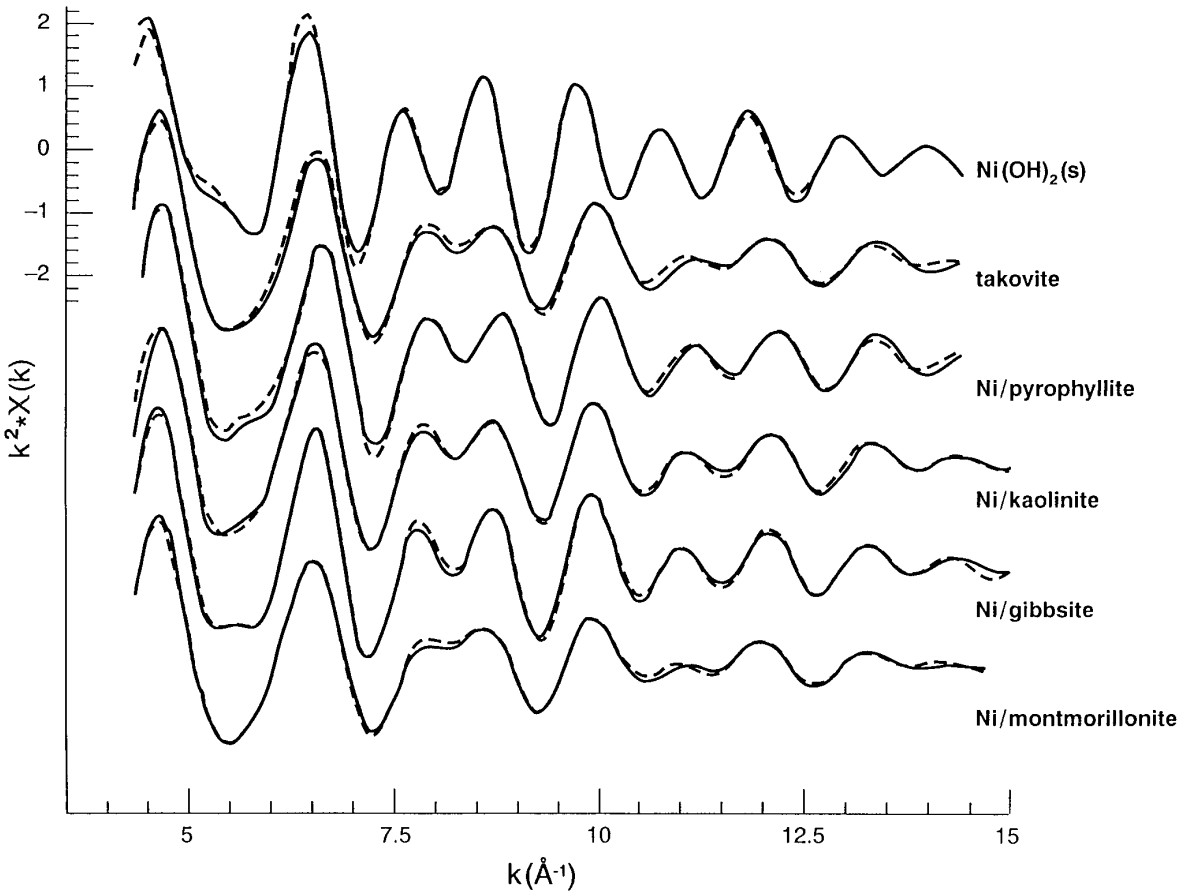

FIG. 7. k^2-Weighted XAFS functions (solid line) for the Fourier back-transformed spectra of Ni sorbed on pyrophyllite, kaolinite, gibbsite, and montmorillonite, and $Ni(OH)_2$(s) and takovite. The theoretical spectra were derived with parameters from analysis of the isolated shells (dashed line).

$Ni(OH)_3^-$ are low (<0.1%). Further details on the speciation are given elsewhere (15).

The appearance of a second shell is consistent with the results from previous XAFS studies on Co sorption on aluminum oxides and clays. The onset of multinuclear complex formation on external sites was observed at coverages as low as 5–10% (12–14). A previous XAFS study of Ni sorption on pyrophyllite suggested the presence of polynuclear surface complexes at low sorption densities; e.g., $\Gamma = 0.49$ μmol m^{-2} (15). If the closest-packing of NiO_6 polyhedra is assumed to constitute a monolayer of Ni atoms, $\Gamma = 0.49$ μmol m^{-2} corresponds to <5% of monolayer coverage.

In the present study the sorption densities were fairly high (e.g., $\Gamma = 3.1$ μmol m^{-2} for Ni on pyrophyllite; Table 1). The sorption densities, Γ's, correspond to a 30% monolayer coverage for pyrophyllite, a double-monolayer coverage for kaolinite, and a 50% monolayer coverage for gibbsite and montmorillonite. The coverage for montmorillonite was estimated based on a 16 m^2 g^{-1} edge surface area of the clay (14).

Structural environment of Ni sorption samples. An important finding of the study is that the structural environment of Ni in all Ni sorption samples is similar. There is also an obvious similarity among the spectra of the Ni sorption samples and the spectrum of tacovite, our mixed Ni/Al hydroxide reference compound, thus suggesting the presence of Ni phases of similar structure.

The existence of mixed-cation hydroxide phases has been reported in the literature (34, 37–42). These compounds consist of structures in which divalent and trivalent metal ions are randomly distributed within the same brucite-like octahedral hydroxide layer. The general chemical formula for the compounds is $[Me^{2+}_{1-x}Me^{3+}_{x}(OH)_2]^{+x}\cdot(x/n)A^{-n}\cdot mH_2O$, where, for example, Me^{2+} is Mg(II), Ni(II), Co(II), Zn(II), Mn(II), and Fe(II), and Me^{3+} is Al(III), Fe(III), and Cr(III). The compounds exhibit a net positive charge x per formula unit which is balanced by an equal negative charge from interlayer anions A^{-n} such as Cl^-, Br^-, I^-, NO_3^-, OH^-, ClO_4^-, and CO_3^{2-}; water molecules occupy the remaining interlayer space (38–41). The octahedral layers can be stacked with hexagonal symmetry and two layers per unit cell, with rhombohedral symmetry and three layers per unit cell, or with less symmetrical arrangements (40). Minerals with the chemical formula given above are classified as the pyroaurite–sjoegrenite group (41). Natural pyroaurite and sjoegrenite are polymorphs having the composi-

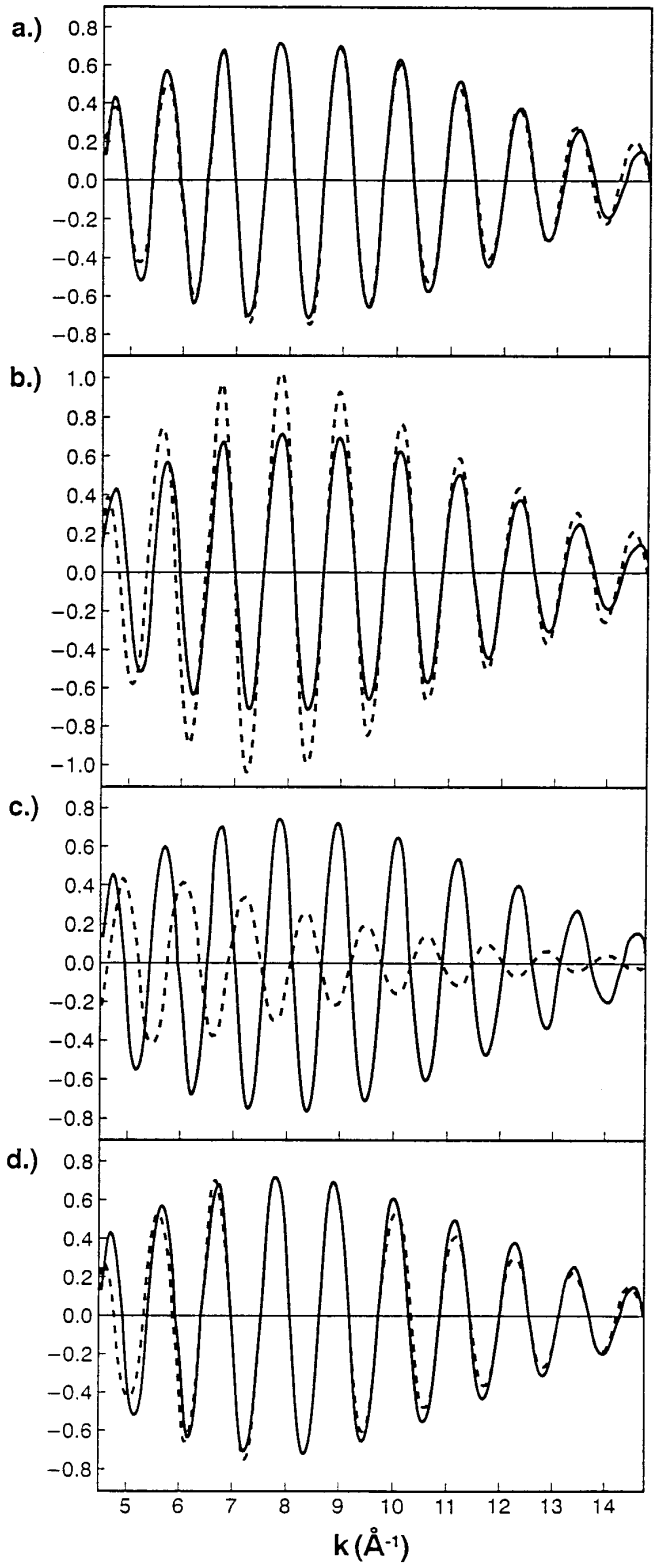

FIG. 8. k^2-Weighted filtered experimental XAFS spectra (solid line) and theoretical spectra (dashed line) of the second RSF peak of the Ni/pyrophyllite sample. (a) Fit assuming Ni and Si or Al. (b) Fit showing only the contribution of Ni. (c) Fit showing only the contribution of Si or Al. (d) Best fit incorporating only Ni as second backscatterer atoms.

tion $Mg_6Fe_2(OH)_{16}CO_3 \cdot 4H_2O$. The minerals takovite, $Ni_6Al_2(OH)_{16}CO_3 \cdot H_2O$, and hydrotalcite, $Mg_6Al_2(OH)_{16}CO_3 \cdot H_2O$, are among the most common natural mixed-cation hydroxide compounds containing Al (39).

The synthesis of mixed-cation hydroxide compounds. The synthesis of mixed-cation hydroxide compounds can be performed by induced hydrolysis (39). When a suspension of a fully hydrolyzed cation is added to a solution of another cation and the pH is maintained constant and slightly below the value at which the second cation hydroxide would precipitate, hydrolysis of the solution cation and the precipitation of the fully hydrolyzed mixed-cation hydroxide compound occurs. In our study all experimental requirements for the formation of mixed-cation hydroxide compounds were fulfilled. Al was the fully hydrolyzed cation (see discussion below), Ni was the second cation, and the pH was maintained constant with the pH-stat apparatus at about 0.5 pH units below the pH where the precipitation of $Ni(OH)_2$ would be expected in homogenous solution (17).

In the literature mixed Ni/Al compounds have been synthesized containing Cl^-, Br^-, OH^-, ClO_4^-, and CO_3^{2-} (38–41). In our systems the anions present were NO_3^- and OH^- (NaOH was used to maintain a constant pH). We could not detect dissolved Al in our samples, a necessity for the formation of mixed Ni/Al compounds. Even so, Al could have been released into solution and incorporated into mixed (Al, Ni) hydroxides. Indeed, the macroscopic data presented in Figs. 2 and 3 suggest that surface complexes of Ni on kaolinite and pyrophyllite destabilize surface metal ions (Al and Si) relative to the bulk solution, and therefore lead to an enhanced dissolution of the clay. The association of Ni with Al could explain why the enhanced dissolution rate is only observable where Ni sorption is pronounced (see Fig. 2).

Mixed Ni/Al hydroxide compounds have been synthesized from Ni and Al salts with initial Ni/Al ratios of 2.5–8 (39, 42). We tried to estimate ''initial Ni/Al ratios'' based on the solution data presented in Figs. 2 and 3. The Ni-sorbed/Si-dissolved ratios for the Ni/kaolinite and the Ni/pyrophyllite systems were approximately 20 and 10, respectively (Figs. 2 and 3). Assuming stoichiometric dissolution of the clays, the amount of released Al is about 20 times smaller than the amount of sorbed Ni for both systems. However, the estimation procedure is problematic for the following reasons. The dissolution of silicates is often incongruent; that is, the stoichiometric ratio of elements released into the solution is not the same as that found in the bulk phase of the mineral (29–31, 43–44). Incongruent dissolution seems to be especially pronounced during the initial dissolution stage (43). For example, kaolinite dissolution was found to be incongruent up to 1000 h, where Al was removed preferentially over Si from the mineral–solution interface from pH 2 to 9 (31). Furthermore, it is known that layered structures of the pyroaurite–sjoegrenite group minerals possess the

unusual property of permanent positive charge that is manifested as a high anion exchange capacity (16). In our case such a high anion exchange capacity could cause $SiO(OH)_3^-$ to be removed from solution and incorporated into the mixed Ni/Al hydroxide phase as an interlayer anion. Thus, the amount of total Si released during the experiments could be larger than the amount Si measured in solution (see Figs. 2–4).

We suspect that in our samples the mixed cation hydroxide phases were formed on the mineral surfaces, rather than as a separate phase. A previous study using high-resolution transmission electron microscopy (HRTEM) revealed distinct alteration in the surface structure of pyrophyllite after reaction with Ni at pH 7.5 (17). Rough, scalloped ''cauliflower-like'' surface deposits were observed occurring preferentially along the edges.

The kinetics of mixed Ni/Al hydroxide formation and Ni sorption. The kinetics of mixed Ni/Al hydroxide formation depend on the pH, the initial Ni/Al ratios in solution, and the anions present (38, 39). For example, a kinetic study revealed that a higher initial Ni/Al ratio in solution resulted in a distinctly slower formation of mixed Ni/Al hydroxides. An increase of the initial Ni/Al ratio from 4 to 8 slowed the reaction down by a factor of ~4 (39). Generally, a reaction time between 1–10 h was required for the formation of mixed Ni/Al hydroxides to be completed at 278K (39). In our study the reaction time was much longer (51–200 h) and in case of Ni sorption on montmorillonite and gibbsite the reaction was not completed. This finding indicates that the release of Al into solution rather than the nucleation process is the rate controlling factor for the formation of mixed Ni/Au hydroxides in our samples. The kinetic data in Fig. 1 reveal that Ni sorption on montmorillonite and gibbsite is distinctively slower than on pyrophyllite and kaolinite. The slower sorption kinetics is in agreement with the slower dissolution reaction of these minerals at pH 7.5 (see Results). However, it must be realized that other factors such as the surface morphology of the sorbents and the impurities present also effect the rate of nucleation processes (43).

It must also be realized, however, that in addition to being incorporated in mixed Ni/Al hydroxide compounds, Ni can bind specifically to Al–OH and Si–OH sorption sites (pyrophyllite, kaolinite, gibbsite, and montmorillonite) and nonspecifically to internal permanent-charge sites (montmorillonite). In the case of Ni sorption on pyrophyllite, bidendate binding of Ni to nonbridging Al–OH surface sites has been suggested as a possible sorption mode (15). A previous XAFS study on Co sorption on montmorillonite revealed, that both outer-sphere, mononuclear surface complexes with internal permanent-charge sites and specific bound, mononuclear Ni complexes with surface hydroxyl sorption sites can occur (14). Preliminary results from a time-resolved spectroscopic study on Ni sorption on clay minerals in our laboratory suggest that mononuclear Ni surface complexation is a fast process, occurring mainly during the first few minutes of the experiment. In comparison with mononuclear Ni surface complexation, the formation of mixed Ni/Al hydroxide compounds is slower, occurring over the entire course of the experiment, and it seems to be predominantly controlled by the dissolution rate of the clay (see discussion above).

Ni/Al ratios in the Ni sorption phase. Table 1 reveals the Ni/Al ratios in the Ni solid phase ($N_{(Ni-Ni)}/N_{(Ni-Si/Al)}$) as deduced by data analysis (Table 1). The XAFS data suggest a Ni/Al ratio of 2.8 for takovite. This is a ratio commonly found in natural takovites (2.5–2.8 (34)). The Ni/Al ratios for the Ni sorption samples are 1.4–2.7 (Table 1) and within the range (1–5.6) observed in synthesized Ni/Al hydroxide compounds (39, 40). However, it must be realized that specific and nonspecific Ni binding to the mineral surface contributes to the overall $N_{(Ni-Si/Al)}$ and decreases the total $N_{(Ni-Ni)}/N_{(Ni-Si/Al)}$ ratio. Our study suggests that this is especially important for the Ni/montmorillonite system, which shows the smallest $N_{(Ni-Ni)}/N_{(Ni-Si/Al)}$ ratio (1.4, Table 1). Indeed, the data from the kinetic studies reveal that most of the Ni in the XAFS sample is sorbed within the first minutes (Fig. 4). During this time period mononuclear Ni surface complexation seems to be an important sorption mode (see ''The kinetics of mixed Ni/Al hydroxide formation and Ni sorption'' above).

Brindley and Kikkawa (40) studied the influence of the Ni/Al ratio in synthesized mixed Ni/Al hydroxide compounds on the lattice parameter *a* of the hexagonal unit cell using XRD. When the Ni/Al ratio in the solid phase decreased from 5 to 2, the lattice parameter *a* decreased from 3.05 to 3.02 Å. The observed change could be explained with a linear relation between the lattice parameters *a*, and the composition of the solid solution alloys expressed as atomic percentage (40). Assuming second-neighbor Ni–Ni backscattering in the present study to be completely caused by Ni–Ni interactions within mixed Ni/Al hydroxide-like phases, the above mentioned linear relation can be used to estimate the Ni/Al ratios based on the Ni–Ni bond distances. Accordingly, Ni–Ni distances between 3.00 and 3.03 Å reflect Ni/Al ratios of 1.8 (pyrophyllite), 2.1 (kaolinite), 2.4 (gibbsite), and 2.8 (montmorillonite). These ratios correspond well with the experimental $N_{(Ni-Ni)}/N_{(Ni-Si/Al)}$ ratios except for the Ni/montmorillonite sample (Table 1).

Comparison with other metal sorption studies on clay minerals and aluminum oxides. An important characteristic of our results is the reduction of the Ni–O and Ni–Ni bond distances compared with those in $Ni(OH)_2$. Such a reduction of bond distances in polynuclear surface complexes in comparison with those found in the pure metal hydroxide, is commonly observed in the literature and has been the objective of intense discussion (12–15, 45, 46). It is useful to compare our findings with XAFS results of Co sorption on kaolinite, montmorillonite, γ-Al_2O_3, and quartz (9, 12–14, 46). In all of these studies polynuclear surface

complexes were detected. Derived Co–Co distances (R = 3.10–3.12 Å in kaolinite (12), 3.12 Å in montmorillonite (14), 3.14 Å in γ-Al_2O_3 (9), and 3.11–3.12 Å in quartz (46) were 0.03–0.07 Å shorter than in crystalline $Co(OH)_2$(s). For the Co–kaolinite system, multinuclear Co(II) hydroxy-like complexes growing epitaxially on the (001) aluminol sheet of kaolinite were suggested (12). However, the model was criticized by other investigators for not providing any conclusive explanation for the reduction of the Co–Co distances relative to an ideal $Co(OH)_2$(s) and the results were alternatively explained by the neoformation of hydrous silicates (45). The specific feature of the clay-like structures is the combination of a Me–Me (e.g., Me = Co(II), Ni(II), Mg(II)) distance between 3.0 and 3.12 Å and the presence of a Si/Al shell near 3.2–3.3 Å (45).

In our study, we strongly doubt that the so-called neoformation of clays is an important sorption mode for the following reasons:

(a) If a significant amount of Ni would form clay-like structures with silicates, one would expect to see a decrease in the release rate of Si during Ni sorption in comparison with the Si release rate of the clay alone. However, this study suggested an increase.

(b) The data show no indication of a shell between or near 3.2–3.3 Å and suggest instead a single Ni–Al/Si distance (3.02–3.07 Å).

(c) The XAFS spectra and derived structural parameters suggest a similar atomic environment for all Ni sorption samples. Neoformation of hydrous silicates can therefore be excluded since such phases cannot be formed upon Ni sorption on gibbsite.

Another mechanism which has been proposed to explain the reduction of the metal–metal distances in a solid as compared to that of the pure metal hydroxide is the formation of hydrogen bonding between adjacent layers (i.e., brucitic sheet in chlorite, Ni–asbolane) (45). The authors, however, argued that in the case of Co sorption on kaolinite, the shortening of the Co–Co distance can hardly be caused by the formation of hydrogen bonds between adjacent layers. Inner-surface hydrogen atoms in kaolinite are pointing away from the aluminol sheet, and this makes the formation of hydrogen bonds with multinuclear cobalt hydroxide complexes difficult (45). A similar argument can be used to discount the formation of hydrogen bonding between adjacent layers in our study.

Additional possible reasons for the contraction of Co–Co distances mentioned in the literature are edge effects from the small particle size of polynuclear surface complexes, the formation of a different metastable phase of $Co(OH)_2$(s), and in the case of Co sorption on quartz, the incorporation of small amounts of Si, molecular water, Na^+, and NO_3^- (from the background electrolyte solution) into the Co–hydroxide structure (46).

We suspect that the formation of a mixed-cation hydroxide-like phase is also a plausible explanation for the reduction of Co–Co distances. Similar to our study, Co–Co distances agree well with those in synthesized mixed Co–Al hydroxide phases (3.12 Å; (38)). Furthermore, at sorption densities where the presence of multinuclear Co complexes were depicted, derived Co/Al,Si ratios varied between 2 and 3, a ratio also observed in synthesized mixed Co–Al hydroxide compounds (39).

CONCLUSIONS

In view of the spectroscopic and kinetic data presented, there is little doubt that mixed-cation hydroxide compounds can be formed in systems containing heavy metals and clay and oxide surfaces. All that is required for the formation of mixed-cation hydroxide compounds is that one cation be introduced into a suitable environment in which there is a source of hydrolyzed species of the second cation. The key factor controlling their formation is that the ionic radius of both metal ions are similar (16, 38). Therefore, we suspect that the formation of mixed-cation hydroxide compounds represents also a plausible ''sorption mode'' in sorption experiments containing divalent metal ions such as Mg(II), Co(II), Zn(II), and Mn(II) and Al(III)-, Fe(III)-, and Cr(III)-(hydr)oxide minerals. To what extent mixed-cation hydroxide compounds actually do form in aquatic and terrestrial environments is probably limited more by slow rates of soil mineral dissolution, a necessary preliminary step, than by lack of thermodynamic favorability (16).

One can speculate that the formation of mixed-cation hydroxide-like phases may be one mechanism responsible for the so called ''aging effect'' observed in many metal sorption experiments (3, 5, 6, 47–52). Desorption experiments have shown that metal release from Ni surface precipitates on pyrophyllite, in this study now identified as a mixed Ni/Al hydroxide phase, is much slower than the dissolution of the crystalline $Ni(OH)_2$(s) reference compounds (18). This finding demonstrates the low solubility of mixed-cation hydroxide phases, and reflects the potential effect of mixed-cation hydroxide formation on the bioavailability, mobility, and the fate of metals in soil and water environments.

Further research is needed to ascertain the conditions of pH, concentration, and temperature and gaseous environment which will affect the rate of the reaction, the degree of crystallinity, and the purity of the phases formed. In addition, we suggest that the formation of mixed-cation hydroxides be considered in metal surface complexation modeling, metal speciation, and risk assessments for the migration of contaminants in polluted sites.

ACKNOWLEDGMENTS

We thank Cathy Olsen for the ICP measurements and Dan Strawn and John DiVincenzo for their careful reading of the manuscript. We gratefully acknowledge the support of this research by the DuPont Company.

REFERENCES

1. Sparks, D. L., ''Environmental soil chemistry.'' Academic Press, San Diego, 1995.
2. Kinniburgh, D. G., and Jackson, M. L., *in* ''Adsorption of inorganics at the solid–liquid interface'' (M. A. Anderson and A. J. Rubin, Eds.), Chap. 3. Ann Arbor Science, Ann Arbor, MI, 1981.
3. Benjamin, M. M., and Leckie, J. O., *J. Colloid Interface Sci.* **79,** 209 (1981).
4. Dzombak, D. A., and Morel, F. M. M., *J. Colloid Interface Sci.* **112,** 588 (1986).
5. Brümmer, G. W., Gerth, J., and Tiller, K. G., *Soil Sci.* **39,** 37 (1988).
6. Davis, J. A., Fuller, C. C., and Cook, A. D., *Geochim. Cosmochim. Acta* **51,** 1477 (1987).
7. Sposito, G., *in* ''Geochemical Processes at Mineral Surfaces'' (J. A. Davis and K. F. Hayes, Eds.), pp. 217–228. ACS Symposium Series 323, American Chemical Society, Washington, DC, 1986.
8. Charlet, L., and Manceau, A., *J. Colloid Interface Sci.* **148,** 443 (1992).
9. Chisholm-Brause, C. J., O'Day, P. A., Brown, G. E., Jr., and Parks, G. A., *Nature* **348,** 528 (1990).
10. Chisholm-Brause, C. J., Roe, A. L., Hayes, K. F., Brown, G. E., Jr., Parks, G. A., and Leckie, J. O., *Geochim. Cosmochim. Acta* **54,** 1897 (1990).
11. Fendorf, S. E., Lamble, G. M., Stapleton, M. G., Kelley, M. J., and Sparks, D. L., *Environ. Sci. Technol.* **28,** 284 (1994).
12. O'Day, P. A., Brown, G. E., Jr., and Parks, G. A., *J. Colloid Interface Sci.* **165,** 269 (1994).
13. O'Day, P. A., Parks, G. A., and Brown, G. E., Jr., *Clays Clay Miner.* **42,** 337 (1994).
14. Papelis, C., and Hayes, K. F., *Colloids Surf.* (in press).
15. Scheidegger, A. M., Lamble, G. M., and Sparks, D. L., *Environ. Sci. Technol.* **30,** 548 (1996).
16. McBride, M. B., ''Environmental chemistry of soils.'' Oxford University Press, New York, 1994.
17. Scheidegger, A. M., Fendorf, M., and Sparks, D. L., *Soil Sci. Soc. Am. J.* **60,** 1763 (1996).
18. Scheidegger, A. M., and Sparks, D. L., *Chem. Geol.* **132,** 157 (1996).
19. Puls, R. W., and Bohn, H. L., *Soil Sci. Soc. Am. J.* **52,** 1289 (1988).
20. Schulthess, C. P., and Huang, C. P., *Soil Sci. Soc. Am. J.* **54,** 679 (1990).
21. Sposito, G., ''The surface chemistry of soils.'' Oxford University Press, New York, 1984.
22. Evans, B. W., and Guggenheim, S., *Rev. Mineral.* **19,** 225 (1988).
23. Eick, M. J., Bar-Tal, A., Sparks, D. L., and Feigenbaum, S., *Soil Sci. Soc. Am. J.* **54,** 1278 (1990).
24. Zhang, Z. Z., Sparks, D. L., and Pease, R. A., *Soil Sci. Soc. Am. J.* **54,** 351 (1990).
25. Carter, D. L., Heilman, M. D., and Gonzalez, C. L., *Soil Sci.* **100,** 356 (1965).
26. Stern, E. A., and Heald, S. M., *Rev. Sci. Instrum.* **50,** 1579 (1979).
27. Lytle, F. W., Greegor, R. B., Sandstorm, D. R., Marques, E. C., Wong, J., Spiro, C. L., Huffman, G. P., and Huggins, F. E., *Nucl. Instr. Methods* **226,** 542 (1984).
28. Gurman, S. J., Binsted, N., and Ross, I., *J. Phys. C* **19,** 1845 (1986).
29. Stumm, W., and Morgan, J. J., (Eds.) ''Aquatic Chemistry.'' Wiley & Sons, New York, 1992.
30. Wieland, E., and Stumm, W., *Geochim. Cosmochim. Acta* **56,** 3339 (1992).
31. Carroll-Webb, S. A., and Walther, J. V., *Geochim. Cosmochim. Acta* **52,** 2609 (1988).
32. Furrer, G., Zysset, M., and Schindler, P. W., *in* ''Geochemistry of Clay-Pore Fluid Interactions'' (D. A. C. Manning, P. L. Hall, and C. R. Hughes, Eds.), p. 243. Chapman & Hall, London, 1993.
33. Heydemann, A., *Geochim. Cosmochim. Acta* **30,** 995–1035 (1966).
34. Bish, D. L., and Brindley, G. W., *Am. Mineral.* **62,** 458 (1977).
35. Manceau, A., and Calas, G., *Clay Miner.* **21,** 341 (1986).
36. Brindley, G. W., and Chin-Chun Kao, *Phys. Chem. Miner.* **10,** 187 (1984).
37. Feitknecht, W., *Helv. Chim. Acta* **25,** 555 (1942).
38. Allmann, R., *Chimia* **24,** 99 (1970).
39. Taylor, R. M., *Clay Miner.* **19,** 591 (1984).
40. Brindley, G. W., and Kikkawa, S., *Am. Mineral.* **64,** 836 (1979).
41. Hashi, K., Kikkawa, S., and Koizumi, M., *Clays Clay Miner.* **31,** 152 (1983).
42. Titulaer, M. K., Jansen, J. B. H., and Geus, J. W., *Clays Clay Miner.* **42,** 249 (1994).
43. Nagy, K. L., *Rev. Mineral.* **31,** 173 (1995).
44. Acker, J. G., and Bricker, O. P., *Geochim. Cosmochim. Acta* **56,** 3092 (1992).
45. Charlet, L., and Manceau, A., *Geochim. Cosmochim. Acta* **58,** 2577 (1994).
46. O'Day, P. A., Chisholm-Brause, C. J., Towle, S. N., Parks, G. A., and Brown, G. E., Jr., *Geochim. Cosmochim. Acta*, **60,** 2515 (1996).
47. Ainsworth, C. C., Pilon, J. L., Gassmann, P. L., and van der Sluys, W. G., *Soil Sci. Soc. Am. J.* **58,** 1615 (1994).
48. Barrow, N. J., Gerth, J., and Brümmer, G. W., *Soil Sci.* **40,** 437 (1989).
49. Kuo, S., and Mikkelse, D. S., *Plant Soil* **56,** 355 (1980).
50. Padmanabham, M., *Aust. J. Soil Res.* **21,** 309 (1983).
51. Lehmann, R. G., and Harter, R. D., *Soil Sci. Soc. Am. J.* **48,** 769 (1984).
52. Schultz, M. F., Benjamin, M. M., and Ferguson, J. F., *Environ. Sci. Technol.* **21,** 863 (1987).